tvst

Article

Clinical 3D Imaging of the Anterior Segment With Ultrasound Biomicroscopy

Richard W. Helms[1], Ahmed Tahseen Minhaz[2], David L. Wilson[2,3], and Faruk H. Örge[1]

[1] Center for Pediatric Ophthalmology and Adult Strabismus, Rainbow Babies and Children's Hospital, University Hospitals Cleveland Medical Center, Cleveland, OH, USA
[2] Department of Biomedical Engineering, Case Western Reserve University, Cleveland, OH, USA
[3] Department of Radiology, Case Western Reserve University, Cleveland, OH, USA

Correspondence: Faruk H. Örge, Rainbow Babies and Children's Hospital, 11100 Euclid Avenue, Cleveland, OH 44106, USA. e-mail: faruk.orge@uhhospitals.org

Received: October 14, 2020
Accepted: January 17, 2021
Published: March 11, 2021

Keywords: ophthalmology; imaging; ultrasound; UBM; three-dimensional; anterior chamber; image processing

Citation: Helms RW, Minhaz AT, Wilson DL, Örge FH. Clinical 3D imaging of the anterior segment with ultrasound biomicroscopy. Trans Vis Sci Tech. 2021;10(3):11, https://doi.org/10.1167/tvst.10.3.11

Purpose: Ultrasound biomicroscopy (UBM) is an important ophthalmic imaging modality due to its ability to see behind pigmented iris and to visualize anterior chamber when the eye's transparency is compromised. We created a three-dimensional UBM (3D-UBM) system and acquired example images to illustrate its potential.

Methods: A commercial 50-MHz two-dimensional UBM (2D-UBM) system was attached to a precision translation stage and translated across the eye to acquire an image volume. The stage was mounted on a surgical microscope, which enabled safe, stable positioning. Image processing steps included image alignment, noise reduction, and calibration. 3D visualization included alignment of the optic axis, multiplanar reformatting at arbitrary orientations, and volume rendering with optimized transfer functions. Scans were performed on cadaver and rabbit eyes.

Results: 3D-UBM allowed visualization of the anterior segment tissues within a 3D anatomical context, unlike 2D-UBM. En face views and interactive slicer operations suggested an ability to plan and assess treatments, including lens placement and microcatheter cannulation of Schlemm's canal. Interactive software allowed us to make accurate measurements of tissue structures (e.g., iridocorneal angles, cyst volumes). In addition, unique measurements of ciliary tissues included single ciliary process volumes of 0.234 ± 0.093 mm^3 with surface areas of 3.02 ± 1.07 mm^2 and ciliary muscle volume of 67.87 mm^3.

Conclusions: 3D-UBM imaging of the anterior segment can be used to enable unique visualization and quantification of anterior segment structures.

Translational Relevance: 3D-UBM provides informative 3D imaging of tissues in the eye that are invisible to light to potentially provide physicians with improved diagnosis, treatment planning, and treatment assessment as compared to conventional 2D-UBM.

Introduction

Ultrasound is widely used in ophthalmology due to its ability to penetrate opaque tissues such as the iris and to visualize deeper and intraocular structures when corneal opacity is compromised due to injury or disease. Clinical ophthalmic ultrasound systems utilize frequencies from about 10 MHz to 50 MHz. High-frequency systems provide higher resolution but limited penetration, making ultrasound biomicroscopy (UBM) systems ideal for imaging the front part of the eye. UBM is used in a variety of conditions.[1–3] In an extensive review, He et al.[1] argued that UBM can be used for imaging conditions in the "adnexal, conjunctiva, scleral, corneal, anterior chamber to anterior vitreous and retina," but that a major contribution is in the anterior segment, particularly for glaucoma diagnosis and staging (e.g., pupillary occlusion, congenital glaucoma, primary angle-closure, secondary angle-closure) and glaucoma surgeries (e.g., iridotomy, cyclophotocoagulation, trabeculectomy, shunts). A 2016 review included cysts and tumors, but again highlighted

glaucomatous conditions requiring UBM diagnosis.[2] Although optical coherence tomography (OCT) can provide better images of certain structures (e.g., cornea, retina), any structure behind the iris or blocked by opaque media can only be seen by ultrasound technology. Two-dimensional UBM (2D-UBM) imaging allows many biometric measurements that provide details about the relationships among various structures, including anterior chamber depth, anterior chamber width, lens vault, iris curvature, iris root distance, trabecular–ciliary process distance, iris–ciliary process distance, angle measurements (e.g., trabecular–ciliary process angle, angle-opening distance), lens thickness, anterior lens radius of curvature, anterior segment length, and more.[1,4–8]

The utility of three-dimensional (3D) imaging is widely established throughout medicine, and similar benefits are anticipated with 3D-UBM. 3D images allow the observer to see anatomic relationships that may be unclear or misleading in 2D slices. 3D images can be rotated, sliced, and otherwise manipulated to provide the view that best highlights the relevant anatomy. For example, direct coronal view imaging is difficult secondary to the bony rigid orbit obstructing access but can be easily produced from 3D image volumes. With 2D ultrasound, volume measurements must be estimated from a series of cross-sections whose orientation may not be optimal. 3D images can then be segmented to provide direct volume measurements at the voxel level. This is especially important when evaluating structures such as tumors or cysts where accurate volume information informs treatment planning.

3D ophthalmic ultrasound has been applied in the past.[9] The general approach has been to attach a 2D ultrasound probe to a motor that either rotates the probe about an axis through its center (e.g., near the optic axis) or translates it along an axis perpendicular to its image plane.[10,11] In this way, one acquires either an angular set of images or a linear stack. The 3D imaging approach has been utilized to successfully visualize a variety of ophthalmic anatomy and pathologies, including vitreous hemorrhage, choroidal melanoma,[10,12] iris tumor,[11] ciliary body,[13–15] inclusion cysts,[16] and retinoblastoma.[17] OTI Ophthalmic Technologies, Inc. (North York, Ontario, Canada) rotated a low-frequency (12-MHz) 2D probe to obtain a series of diameter images in as little as 2 seconds.[18–21] With low spatial sampling, images were typically viewed in two dimensions rather than three dimensions. We are unaware of any commercially available 3D ophthalmic imaging system available today. In our case, we obtain finely sampled images and use advances in 3D rendering technology to provide high-quality, interactive 3D visualizations.

Anterior segment OCT provides fast, efficient, and high-resolution images via a non-contact system. It has been shown to produce 3D images of the anterior segment but with significantly limited penetration through the iris and sclera in normal eyes. Furthermore, OCT has limited value for patients with opaque media (e.g., opaque cornea, hyphema). Commercially available units currently do not have the standard capability of 3D reconstruction and are limited to tabletop units; thus, they are not portable and cannot be utilized in operating room settings. The commercially available portable or handheld and operating microscope units have limited software capabilities, such that even standard tools (e.g., measurement tools) are not integrated. Also, in many cases, the area of the image acquired is confined to only a small portion of the eye and is geared mostly toward posterior segment applications.

In this report, we share the results of our 3D-UBM imaging system, which utilizes a single-element, linear-scanning, 50-MHz 2D-UBM. This system has a uniform, high-resolution point spread function along the sweep axis, unlike some other systems using a pivoting probe design. As our goal is to investigate high-resolution 3D imaging of structures in the front part of the eye, we designed our system to acquire as many as 1000 image frames, with a spacing of 16-µm between frames. Before illustrating some of the 3D visualizations, we first describe the acquisition system and processing.

Methods

We created 3D-UBM by linear translation of an existing 2D-UBM (Aviso Lin-50; Quantel Medical, Rockwall, TX). This unit consists of a single element transducer that provides a rapid linearly scanned 2D image. The 2D-UBM probe was attached to a linear motion controller, which in turn was attached to a Leica surgical microscope (Leica Microsystems, Wetzlar, Germany) via 3D printed customized attachment parts.

The precise arm of the operating microscope provided accurate, reliable, and safe positioning over the eye with ease. The microscope not only provides a method for securely holding the probe over the patient but also features a multi-axis positioning mechanism that allows adjustment of the position of the probe relative to the eye (Fig. 1). For imaging in other settings, a variety of other 3D-printed adapters

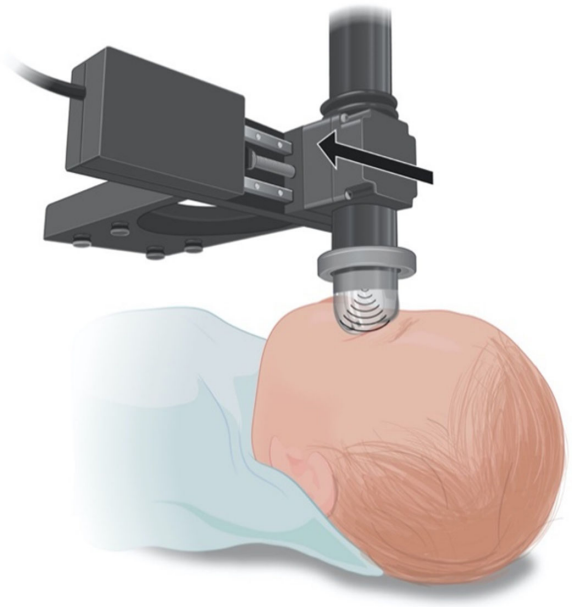

Figure 1. Schematic view of the ultrasound probe attached to the translation stage. The probe and stage are suspended below a surgical microscope (not shown). The probe is coupled to the eye using the ClearScan probe cover and translated across the eye in a direction perpendicular to the probe sweep.

and miscellaneous hardware were used. The probe acquires images in a scan mode, based on starting and ending points of the area that is to be scanned (e.g., limbus to limbus horizontal scan) via the control software. When these two points are given to the software, the software divides the length between the two points in a set number of scans (e.g., 1000 scans) and drives the motor that is moving the probe over the eye at a speed necessary to acquire the number of images between the two points. The 2D-UBM is typically oriented cranial–caudal (y-axis, fast scan), and the linear motion controller continuously moves the 2D-UBM on the x-axis (slow scan) from left to right or right to left, at a constant speed, with depth in the eye along the z-axis. Recorded images are processed by other software that aligns and stacks the images to provide a 3D composite image (Fig. 1). The manufacturer reported that values for the point spread function are 60 µm and 35 µm in x and z, respectively. A 3D acquisition typically consists of 40-µm × 10-µm pixel images with nominal 16-µm spacing (slow x-axis), giving ~1000 2048 × 384 pixel images across a 16-mm anterior segment, giving a volume of view and resolution to image tissues of interest. The scanner was acoustically coupled using a water-filled pliable chamber (ClearScan; ESI, Inc., Plymouth, MN), which provided a safe scanning distance (at >1 cm) from the eye. The technical specifications of the Quantel transducer and the motion controller (MTS50-Z8E; Thorlabs, Newton, NJ) can be found in Tables 1 and 2.

Table 1. Technical Specifications for the Quantel Aviso UBM System

Transducer frequency	50 MHz
Linear transducer movement	16 mm
Focus	9–11 mm
Axial resolution	35 µm
Lateral resolution	60 µm

We imaged both ex vivo (human cadaver) and in vivo (rabbit) eyes. For in vivo experiments, the rabbits were sedated with ketamine and placed on a heated bed. A speculum was used to retract the eyelids. The probe and the translation stage were attached to a flexible arm that was positioned over the rabbit's eye. A ClearScan probe cover was used to acoustically couple the probe to the eye. Lubricating gel was also used to protect the cornea and to allow the ClearScan to move over the cornea with minimal friction. Using a live view, the operator identified the temporal and nasal extent of the desired scan, then initiated the collection of a various number of frames (100 to 500). For ex vivo imaging, the cadaver globe was placed in a 3D-printed eye holder apparatus. During scanning the ClearScan bag was filled with a limited amount of distilled water, so that it would loosely conform to the shape of the cornea. As a result, there was no undue pressure on the eye other than that from the water height in the ClearScan water bag. The 1-cm gap between the transducer end eye ensures that there is no chance of the transducer colliding with the eye during movement. Similar to manual ultrasonography, the distance between the probe tip and the cornea is visualized in real time on the ultrasound screen to ensure accuracy of the imaging depth. Cadaver eye imaging was done with a specialized holder crafted using 3D printing.

We applied several image processing and visualization steps to the data. Image frames were aligned using normalized cross-correlation on a frame-by-frame basis, starting from a center frame. The stack was then linearly filtered to lightly reduce noise using a Gaussian filter. Data were made isotropic using a high-quality (bicubic trilinear) resampling process to create isotropic voxels of 20 µm on each side. Optionally, more aggressive noise reduction was applied (e.g., non-local means filter).[22] Several data visualization steps were applied. Typically, we realigned data along the optic axis to aid intuitive interaction. We used interactive multiplanar reformatting, slicer views, and volume rendering to aid visualizations of specific

Table 2. Technical Specifications for the Thorlabs MTS50-Z8E Linear Motion Controller

Travel range	50 mm
Maximum velocity	2.4 mm/s
Minimum achievable incremental movement	0.05 µm
Bidirectional repeatability	1.6 µm
Backlash	<6 µm

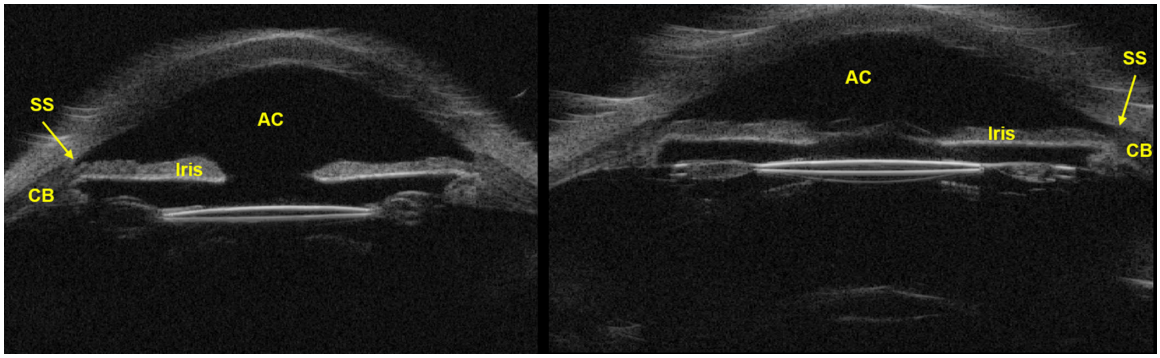

Figure 2. Conventional 2D-UBM images of ex vivo human eye. 2D-UBM allows visualization of important anatomical structures, such as the anterior chamber (AC), scleral spur (SS), iris, and structures posterior to the iris, such as the ciliary body (CB).

tissues.[23] Volume visualization was done using optimized transfer functions. En face visualizations of tissues such as the ciliary body were aided by the fact that the anterior chamber consists of non-echogenic fluid, providing a sharp step edge for rendering. We used Amira software (Thermo Fisher Scientific, Waltham, MA) to assemble the registered, denoised frames into a 3D volume. Color and transparency were adjusted, and unimportant regions were cropped to yield optimal 3D images highlighting the desired structures. Measurements of important tissue structures (anterior chamber, iridocorneal angle, and ciliary body) were made with interactive software.

To verify 3D volumetric measurements, the known dimensions of an implanted intraocular lens (AcrySof single-piece lens; Alcon Laboratories, Geneva, Switzerland) in a cadaver eye were compared with measurements made from the 3D-UBM volume. The optic diameter and IOL thickness were measured at multiple locations from the 3D image and compared with those of the explanted lens.

Results

3D-UBM visualizations, particularly en face views, reveal anatomical details not discernible with 2D-UBM. In Figure 2, we show conventional 2D views that include the posterior iris and ciliary body. In Figure 3, we show 3D en face views of the iris and ciliary body. The lens and cornea have been cropped out to enable unobstructed views of the iris from both anterior and posterior perspectives. The anterior view allows visualization of the iridocorneal angle, and the posterior view shows the ciliary body, including individual ciliary processes. As shown in Supplementary Movie S1, volumes can be interactively rotated in 3D, allowing visualization from any direction. (A narrative in the movie describes how various structures are revealed.) In 2D-UBM (Fig. 2), the images show the cornea, anterior chamber, iris, pupil, iridocorneal angle, scleral spur, ciliary body, and the intraocular lens placed in the capsular bag and centered in the anatomical position. However, the viewer will not be able to discern the condition of the rest of the eye and in which position this image has been acquired (such as 12 o'clock or any other orientation).

The 3D-UBM can be useful in ophthalmological surgical interventions. Figure 4 shows an ex vivo globe with a lens in the capsular bag. Intraocular lenses (IOLs) are hyperechoic compared to adjacent ocular tissueFig, enabling good visualization of the intraocular artificial lens. In this case, the lens has been segmented, and the 3D volume has been cropped to a thin plane to highlight the lens position relative to the posterior iris, ciliary processes, and the bag. In Supplementary Movie S2, we show a segmented IOL placed in the capsular bag. Although individual familiar 2D

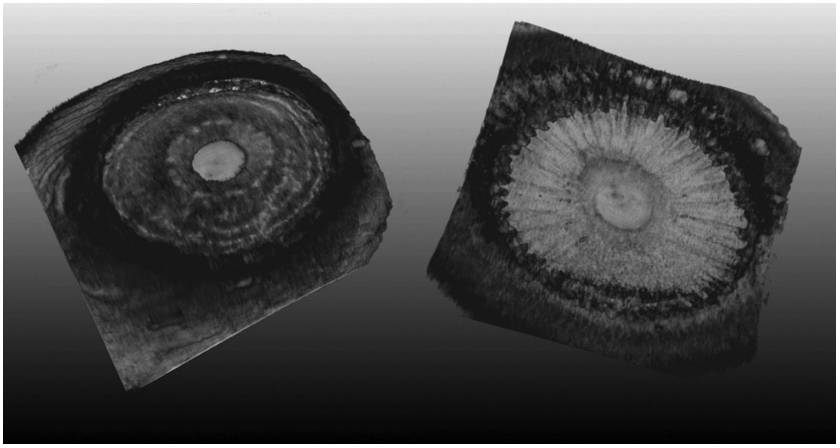

Figure 3. Anterior (*left*) and posterior (*right*) iris in an ex vivo human eye. The anterior cornea is cropped away to provide unobstructed view of the iris from both the anterior and posterior perspective. The anterior view allows complete 360° visualization of the iridocorneal angle. The posterior view allows visualization of the ciliary body, including individual ciliary processes. See Supplementary Movie S1 for an interactive 3D viewing of this eye.

images and slices can also be obtained, the complete 360° view clearly demonstrates the details where the IOL is placed: all of the adjacent tissues, details for each ciliary process, zonules, closeness of the IOL to tissue structures, iridocorneal angle, and many other details that could be important for an anterior segment surgeon.

As another example of surgical intervention, Figure 5 shows a cadaver eye with an iTrack microcatheter (Ellex Medical, Adelaide, Australia) placed in the Schlemm's canal (SC). The iTrack is used in canaloplasty or ab interno canaloplasty procedures to open the canal and increase aqueous outflow. Although the conventional 2D-UBM provides visualization of this device in the SC as a bright spot, there is no way to know if the SC has been cannulized all around the circumference. With interactive visualization of 3D-UBM, we cropped the cornea away and visualized the catheter within the canal in 3D. To improve visualization, we applied semantic segmentation of the catheter. This technique can be used to verify the placement of the catheter and reliably determine the extent of cannulization. Before and after images may help to evaluate the SC and its conditions (patency, location, and morphological changes secondary to the procedure). The ability to segment the IOL and the catheter in the eye demonstrates the potential to apply 3D-UBM to assess the permanent or temporary placement of other hardware within the eye.

3D-UBM allows us to make accurate volumetric measurements that are impossible with 2D-UBM. In Figure 6, we tested our ability to make accurate measurements by comparing measurements from 3D-UBM to known dimensions in an IOL. The measured diameter was 6.04 mm in the fast scan direction and 6.25 mm in the slow scan direction. From measurements at eight different locations around the eye, the lens diameter was measured as 6.14 ± 0.05 mm, with a mean within 2.33% of the actual diameter of 6.0 mm. For depth measurements in tissue, we have found the 3D-UBM system to be as accurate as the underlying 2D-UBM. As an independent test, we measured the thickness of the IOL haptic. We measured 0.28 mm, which was approximately corrected to 0.40 mm based on the speed of sound, giving a value within 7% of the reported thickness of 0.43 mm. The correction was done using the following formula: haptic thickness = (true velocity/assumed velocity) × apparent haptic thickness, using the sound speeds of 2180 m/s and 1532 m/s for acrylic material and tissue, respectively. Our results were quite close, given that the actual speed of sound could be different in the IOL.

Validation of the accuracy of the dimensions opens the possibility of accurate volumetric assessments of various structures in the eye. In Figure 7, we show results from an automated, deep-learning segmentation of the anterior chamber volume, giving 267 mm^3, as compared to 264 mm^3 as measured by an expert using manual pixel-by-pixel segmentation.[23]

Using 3D-UBM, one can image the entire anterior segment, including the anterior chamber and ciliary processes and body, structures that are important in glaucoma. Anterior chamber angle can be manually or automatically measured at any clock

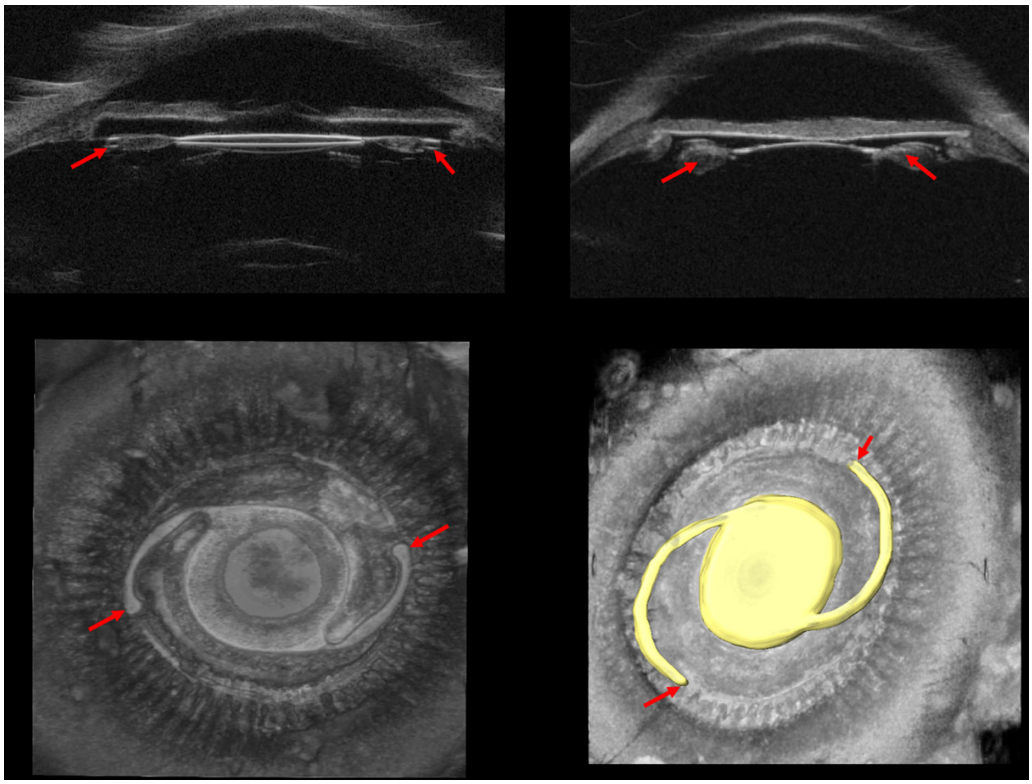

Figure 4. Structures important for treatment planning and assessment are easily visualized. Positioning of IOL using conventional 2D-UBM does not provide any meaningful visualization of the IOL haptics (*red arrow*); shown are an AcrySof single-piece IOL (*top left*) and a three-piece IOL (*top right*). 3D-UBM shows the exact location of IOLs (*bottom right*, *yellow*), location of the haptics (*bottom*, *red arrow*), and condition of surrounding tissues. Supplementary Movie S2 provides an interactive view of IOL haptics enabled by 3D-UBM.

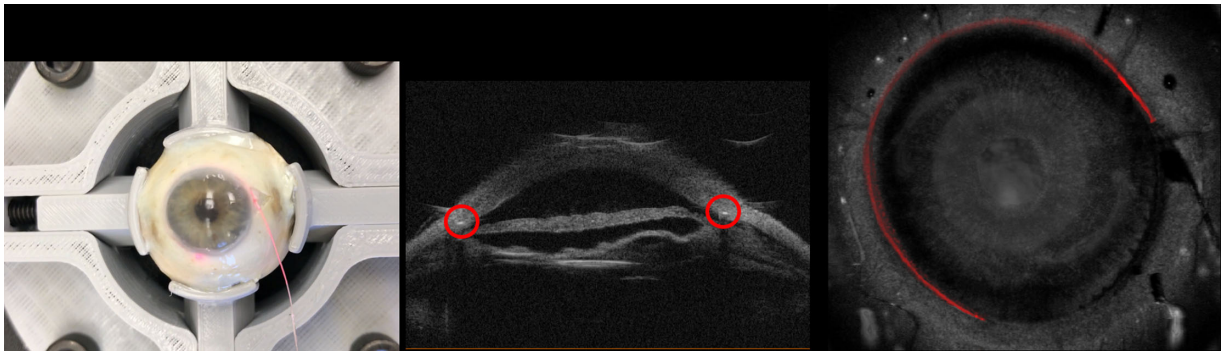

Figure 5. Cadaver eye with iTrack microcatheter placed in Schlemm's canal. (A) Color photograph shows the catheter inserted externally at 3 o'clock and threaded counterclockwise. The tip of the catheter is indicated by a red light emitted from the tip through the sclera. (B) Conventional UBM shows the catheter as a bright spot within the Schlemm's canal. (C) 3D-UBM volume of the same eye with the cornea cropped away and the catheter segmented to show its location within the canal. Between 9 and 1 o'clock, the catheter appears less bright, as it is slightly deeper in the tissue.

orientation. Figure 8 demonstrates a 360° angle heat map of a cadaver eye showing the range of anterior chamber angle. An en face view (Fig. 9) greatly aids the determination of structures nearly impossible to identify in 2D sagittal views. Ciliary muscle and processes are manually segmented, illustrating that we can obtain unique biometrics (Fig. 9). Single process volumes were 0.234 ± 0.093 mm^3, with surface areas adjacent to aqueous humor of 3.02 ± 1.07 mm^2. Ciliary muscle volume was measured at 67.87 mm^3, which is in agreement with the literature.[24] With 3D-UBM, it is possible to visualize and measure cysts and tumors. Figure 10 shows a cadaver eye with a cyst-like formation located near the iris and ciliary body. Its volume was 0.38 mm^3.

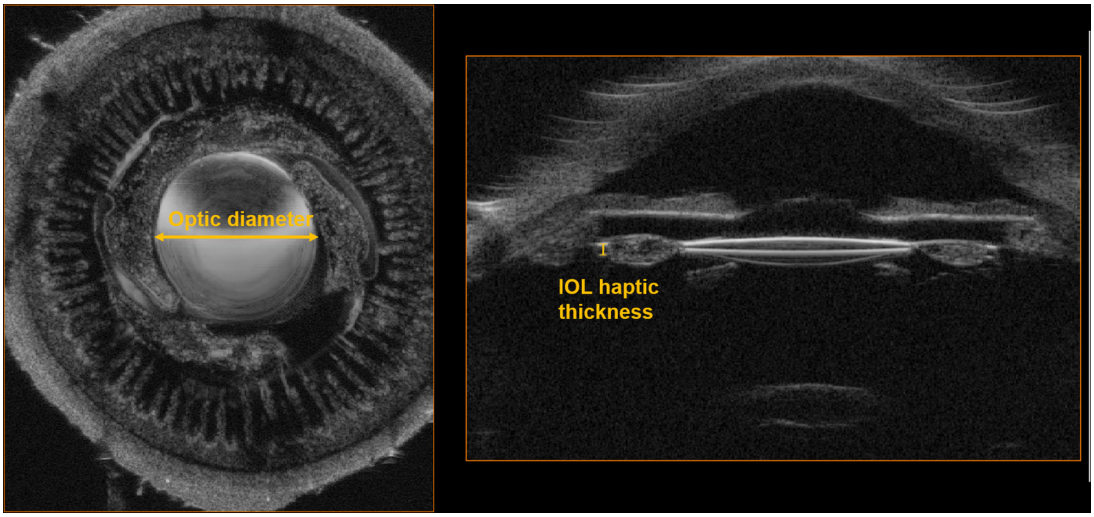

Figure 6. Cadaver eye with an AcrySof single-piece IOL (optic diameter 6 mm, thickness 0.43 mm) confirming dimensions measured in 3D-UBM. The cadaver eye was imaged in 3D, producing the two cross-sections shown above. The size of the lens was measured at eight different locations from the 3D image and compared with that of the explanted lens. Optic diameter was measured at 6.14 ± 0.05 mm (error, 2.33%) and corrected IOL haptic thickness was 0.40 mm (error, 6.97%).

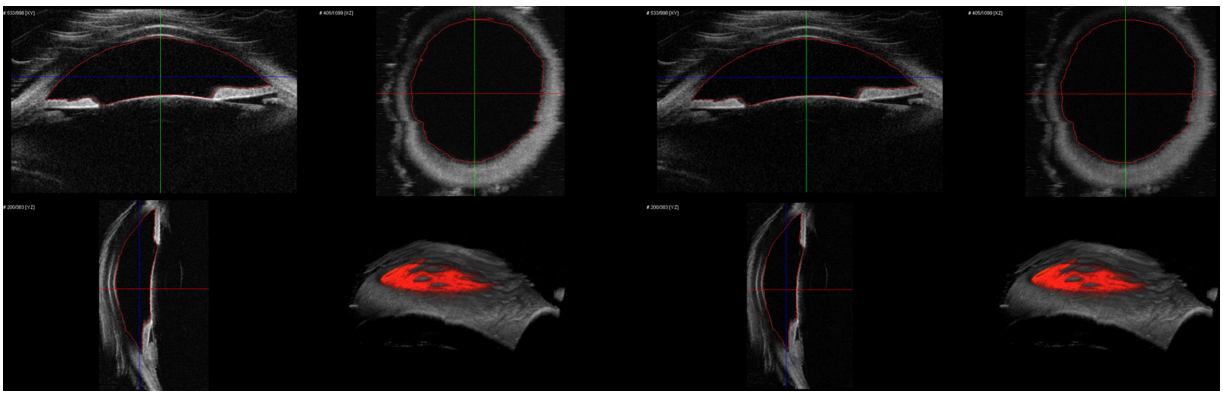

Figure 7. Manual (*left*) and automated (*right*) segmentation of the anterior chamber of a cadaver eye with the boundary in *red*. The anterior chamber volume from the manual segmentation was measured at 264 mm^3; from the fully automated segmentation, it was 267 mm^3.

We have successfully used 3D-UBM to image rabbit eyes in vivo (Fig. 11). Motion was limited, as the rabbits were sedated, and image registration successfully corrected any small motions due to breathing. Figure 11 shows the imaging setup and a segmented anterior chamber with part of the cornea cropped away to aid visualization.

Discussion

Our 3D-UBM provides new, informative views of tissue structure and devices. In particular, en face views reveal structures that cannot be interpreted from conventional 2D-UBM scans (compare Figs. 2 and 9). It is believed that such visualizations will greatly aid clinical interpretations, including tissue anomalies, various disease-related changes, and age-related variations, in addition to revealing the effects of various surgeries on normal structures. There are many clinical examples where seeing the structures can help with clinical decision making. Cataract surgery, the most commonly performed surgery in the world, provides many examples that will be familiar to almost all ophthalmic clinicians. In many cases, the cataractous lens is removed and a man-made IOL is placed in the capsular bag, providing the most anatomically appropriate positioning of the lens. But, in cases where the lens must be placed in the sulcus space, between the capsules and iris, this can lead to unwanted problems, such as lens

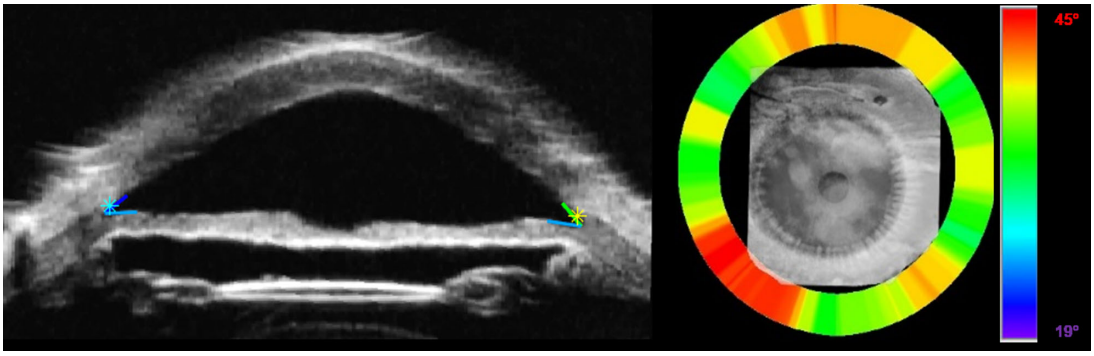

Figure 8. Automated trabecular iris angle (TIA) measurements. (A) Rotational view image with scleral spur and angles identified. (B) Angle heat map showing variation around the eye. Note the tendency for increased angle between 7 and 8 o'clock. The color map depicts angle variations from 19° (*blue*) to 45° (*red*).

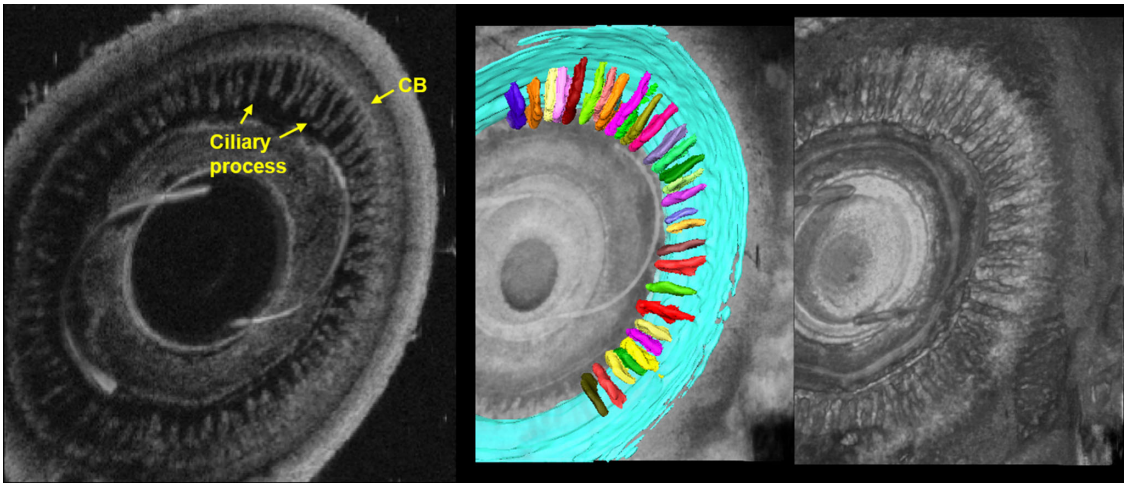

Figure 9. En face view and segmentation of ciliary muscle (*blue*) and ciliary processes (*multicolor*). The en face view allows unique visualization of the ciliary body and processes not possible with conventional 2D-UBM. The anterior–posterior rendering clearly shows the ciliary body. Segmentations reveal the unique 3D biometrics of tissues that are important in glaucoma.

proliferation around the IOL haptics, causing tilt of the lens that induces lenticular astigmatism, as well as scar tissue between the capsule and the iris that leads to chaffing (i.e., uveitis glaucoma hyphema syndrome). Trauma-related or hereditary problems leading to uveal tissue changes, zonular defects, pseudoexfoliaton, cysts behind the iris, and scar tissue formation can only be safely visualized with high-resolution ultrasonography. Similarly, the positions of other implants and devices (e.g., tube shunts and slow medication releasing platforms), scar tissue formation, and other morphological changes secondary to device or implant insertion can only be seen by ultrasonography. Also, there are many anatomical alterations created by routine surgeries that have a direct effect on the physiology of the eye, but the exact mechanisms and quantifiable correlations are not thoroughly understood. In one important example, intraocular pressure (IOP) is known to change secondary to cataract extraction and IOL implantation. Understanding the exact mechanism and relationship of IOP changes and morphological changes created by the surgery can be improved through enhanced and careful visualization of the intermediary structures (i.e., irido–corneal angle, iris plane, ciliary structures, lens, and zonular structures). 2D-UBM is the only readily available technology that is able to visualize the intermediary structures; hence, 3D-UBM should add crucial if not critical further detail to this area (Fig. 4).

3D-UBM offers new opportunities for quantification, and we have shown measurements of the irido-corneal angle (Fig. 8) and unique measurements of the ciliary structures (Fig. 9). Our 3D-UBM system

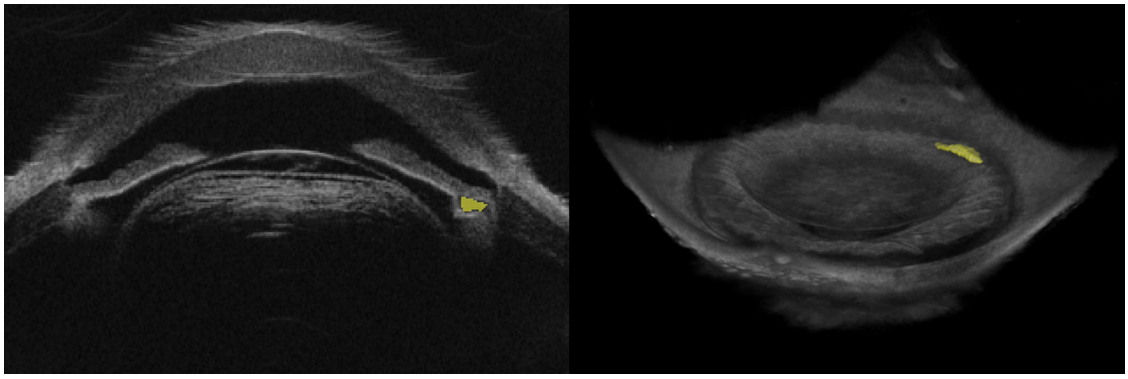

Figure 10. Cadaver eye with cyst-like formation following cyclophotocoagulation (CPC). After application of CPC, the formation (*yellow*) appeared near the iris and ciliary body. The formation was manually segmented, giving a volume of 0.38 mm^3. With 3D-UBM, we can visualize its entire volume and location relative to other anterior segment tissues.

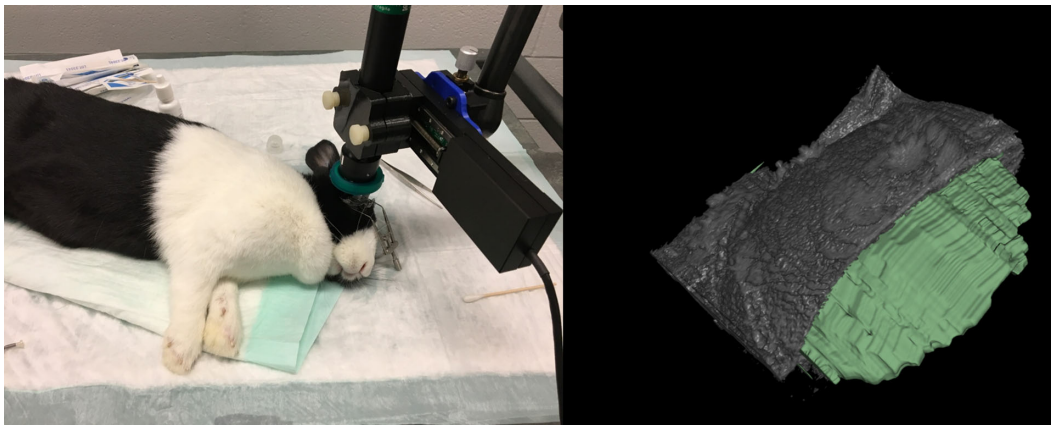

Figure 11. In vivo imaging of rabbit anterior chamber. Rabbits were sedated, and the probe was attached to a flexible arm and positioned over the rabbit's eye. The AC was scanned using 100 frames. The AC was manually segmented (3D Slicer software) to determine AC volume and depth. This figure shows the segmented AC (*green*) with part of the cornea cropped away.

eliminates 2D handheld probe orientation error. In particular, with multiplanar reformatting, one can ensure that the image slice is oriented properly for the measurement (e.g., a proper perpendicular view for the iridocorneal angle). When there was an 8° tilt, the average difference in angles measured between tilted and reformatted data was 12%.[23] Note that any biometric measurement made in 2D (such as trabecular–ciliary process angle, angle-opening distance, trabecular–ciliary process distance, iris–ciliary process distance and iris root distance, as described previously) can be done accurately in multiple positions with 3D images. For example, 3D-UBM has the ability to take many iridocorneal angle measurements and possibly average them. With 2D-UBM, there is potential sampling error when one chooses a single location to evaluate; therefore, 360° angle measurement provides more complete spatial information than can be obtained from traditional 2D-UBM.

3D-UBM will improve current diagnosis and treatment planning that utilizes 2D-UBM. Retrospective 2D studies on glaucoma and lens accommodation[1,4] require that optimal 2D-UBM views be saved, but such studies would be much easier and more accurate with 3D-UBM views. With 3D-UBM, one should be able to reproducibly image tumors and quantify their volumes. This will be important for assessing changes due to therapeutics. 3D-UBM can visualize and determine the precise location of the lens in 3D and the associated anatomy which would aid in initial lens placement, especially in complex cases, and in repairing

lens dislocations. In Figure 6, the difference between actual and measured IOL diameter is within about 2%. The accuracy of a depth measurement is limited only by knowledge regarding the velocity of sound, as in standard 2D ultrasound. It has been shown that 3D-UBM is capable of making accurate measurements of structures within the eye. With 3D-UBM, imaging and volume measurement can be relatively fast and easy. In Figure 10, we segmented a cyst-like formation and measured its volume, thus demonstrating the ability of 3D-UBM to provide intuitive visualization and quantification of cyst or tumor volumes. In oncology, it is now recognized that tumor volume is superior in terms of reproducibility and predictive value as compared to 2D tumor measurements (e.g., RECIST).[25] As with computed tomography and magnetic resonance imaging, volumetric measurements using 3D-UBM will enable more accurate assessment of changes due to treatments (e.g., tumor shrinkage secondary to ablation or chemotherapy).

Although we have focused on anterior segment imaging using a high-frequency UBM transducer, one can also use lower frequency transducers to image the rest of the eye and the structures behind the globe. This could expand the number of applications, including the imaging of posteriorly located intraocular tumors. With the current technology, it can take up to an hour for a skilled ultrasonographer to evaluate intraocular tumors, such as choroidal melanoma, to map the various aspects of the tumor and interpret possible changes in consecutive sessions as the patients are closely followed up by the ocular oncology team. A well-targeted 3D ultrasound scanning the tumor in total will undeniably result in better evaluation of the volume of the tumor. The images obtained by virtually any clinician or appropriate personnel at separate times can be superimposed to assess for even minute changes of a tumor with greater accuracy, ease, and speed.

As compared to conventional 2D imaging, 3D-UBM has a particular advantage regarding image acquisition and interpretation. The acquisition of 2D images requires a skilled operator, preferably an ocular ultrasonographer, but such trained and certified experts are very much in demand, as there are only a few in the nation. After acquisition of 2D images, detailed mappings must be recorded, and the reader must assemble a mental collage of the whole. Image acquisition by sweeping the handheld probe manually at a precise direction and speed without pressing on the eye and manipulating the tissue can be difficult even for an experienced ultrasonographer. With 3D-UBM, ophthalmic personnel with significantly less training will be able to acquire images in any clinical or surgical setting. For 3D-UBM, one easily positions the scanner, sets the beginning and end sweep positions to cover the area intended to be measured, and lets the scanner perform the acquisition. When the volume has been obtained, interactive visualizations will allow a physician to fully evaluate structures of interest in an intuitive fashion. Automation and intuitive visualization can improve results obtained by even inexperienced UBM users, allowing those who are unfamiliar or uncomfortable with UBM imaging to embrace this extremely useful modality. Three-dimensional visualization will likely be particularly valuable for trainees who are still becoming comfortable with normal, let alone pathological, anatomy.

Although preliminary results are promising, there is a challenge with 3D-UBM. Our implementation uses a 2D ultrasound system, which mechanically scans a single element. Frame rates on such systems are typically 12 to 15 frames/s, and this ultimately sets a lower limit on the time for our 3D acquisitions. Currently, our system acquires a 1000-slice image volume in about 2 minutes. Eye movement can be a significant problem in vivo. One solution is to simply apply the technique to subjects under general anesthesia or deep sedation. Under such conditions, it is likely that any residual motion can be robustly corrected using image alignment algorithms, as in our rabbit experiments. One target clinical application is imaging for surgical planning and assessment in pediatric patients, where all patients will be under general anesthesia. For awake patients, 3D-UBM will require greater cooperation of the subject, a well-designed fixation target, speeding up our current process by acquiring fewer images, and advanced alignment processing. Newer technologies that are widely used in clinical practices but not yet available for ophthalmic use, such as linear phased array or plane wave, will enable much faster imaging, enabling rapid 3D acquisitions. This could rapidly expand the usage of ultrasound in ophthalmology.

Acknowledgments

Supported by a Case-Coulter Translational Research Partnership (PY18-P512). This work made use of high-performance computing resources within the Core Facility for Advanced Research Computing at Case Western Reserve University. This research was conducted in space renovated using funds from a National Institutes of Health construction grant

(C06 RR12463) awarded to Case Western Reserve University. The veracity guarantor, Juhwan Lee, affirms to the best of his knowledge that all aspects of this paper are accurate.

Disclosure: **R.W. Helms**, None; **A.T. Minhaz**, None; **D.L. Wilson**, None; **F.H. Örge**, None

References

1. He M, Wang D, Jiang Y. Overview of ultrasound biomicroscopy. *J Curr Glaucoma Pract*. 2012;6(1):25–53.
2. Mannino G, Abdolrahimzadeh B, Calafiore S, Anselmi G, Mannino C, Lambiase A. A review of the role of ultrasound biomicroscopy in glaucoma associated with rare diseases of the anterior segment. *Clin Ophthalmol*. 2016;10:1453–1459.
3. Silverman RH. High-resolution ultrasound imaging of the eye – a review. *Clin Exp Ophthalmol*. 2009;37(1):54–67.
4. Li M, Chen Y, Chen X, et al. Differences between fellow eyes of acute and chronic primary angle closure (glaucoma): an ultrasound biomicroscopy quantitative study. *PLoS One*. 2018;13(2):e0193006.
5. Ramasubramanian V, Glasser A. Objective measurement of accommodative biometric changes using ultrasound biomicroscopy. *J Cataract Refract Surg*. 2015;41(3):511–526.
6. Okamoto Y, Okamoto F, Nakano S, Oshika T. Morphometric assessment of normal human ciliary body using ultrasound biomicroscopy. *Graefes Arch Clin Exp Ophthalmol*. 2017;255(12):2437–2442.
7. He N, Wu L, Qi M, et al. Comparison of ciliary body anatomy between American Caucasians and ethnic Chinese using ultrasound biomicroscopy. *Curr Eye Res*. 2016;41(4):485–491.
8. Qureshi A, Chen H, Saeedi O, et al. Anterior segment ultrasound biomicroscopy image analysis using ImageJ software: intra-observer repeatability and inter-observer agreement. *Int Ophthalmol*. 2019;39(4):829–837.
9. Coleman DJ, Silverman RH, Rondeau MJ, Lizzi FL. New perspectives: 3-D volume rendering of ocular tumors. *Acta Ophthalmol Suppl*. 1992;204:22.
10. Downey DB, Nicolle DA, Levin MF, Fenster A. Three-dimensional ultrasound imaging of the eye. *Eye (Lond)*. 1996;10(1):75–81.
11. Silverman RH, Rondeau MJ, Lizzi FL, Coleman DJ. Three-dimensional high-frequency ultrasonic parameter imaging of anterior segment pathology. *Ophthalmology*. 1995;102(5):837–843.
12. Finger PT, Romero JM, Rosen RB, Iezzi R, Emery R, Berson A. Three-dimensional ultrasonography of choroidal melanoma. *Arch Ophthalmol*. 1998;116(3):305–312.
13. Cusumano A, Coleman DJ, Silverman RH, et al. Three-dimensional ultrasound imaging: clinical applications. *Ophthalmology*. 1998;105(2):300–306.
14. Silverman RH, Lizzi FL, Ursea BG, et al. High-resolution ultrasonic imaging and characterization of the ciliary body. *Invest Ophthalmol Vis Sci*. 2001;42(5):885–894.
15. Stachs O, Martin H, Kirchhoff A, Stave J, Terwee T, Guthoff R. Monitoring accommodative ciliary muscle function using three-dimensional ultrasound. *Graefes Arch Clin Exp Ophthalmol*. 2002;240(11):906–912.
16. Kirchhoff A, Stachs O, Guthoff R. Three-dimensional ultrasound findings of the posterior iris region. *Graefes Arch Clin Exp Ophthalmol*. 2001;239(12):968–971.
17. Finger PT, Khoobehi A, Ponce-Contreras MR, Rocca DD, Garcia JPS. Three dimensional ultrasound of retinoblastoma: initial experience. *Br J Ophthalmol*. 2002;86(10):1136–1138.
18. Garcia JPS, Garcia PMT, Rosen RB, Finger PT. Optic nerve measurements by 3D ultrasound-based coronal "C-scan" imaging. *Ophthalmic Surg Lasers Imaging*. 2005;36(2):142–146.
19. Garcia JPS, de la Cruz J, Rosen RB, Buxton DF. Imaging implanted keratoprostheses with anterior-segment optical coherence tomography and ultrasound biomicroscopy. *Cornea*. 2008;27(2):180–188.
20. Ishikawa H, Schuman JS. Anterior segment imaging: ultrasound biomicroscopy. *Ophthalmol Clin N Am*. 2004;17(1):7–20.
21. Finger PT, Khoobehi A, Ponce-Contreras MR, Rocca DD, Garcia JPS. Three dimensional ultrasound of retinoblastoma: initial experience. *Br J Ophthalmol*. 2002;86(10):1136–1138.
22. Buades A, Coll B, Morel J-M. A non-local algorithm for image denoising. In: *2005 IEEE Computer Society Conference on Computer Vision and Pattern Recognition (CVPR'05)*. Vol. 2. Piscataway, NJ: Institute of Electrical and Electronics Engineers; 2005:60–65.
23. Wu H, Minhaz AT, Helms R, et al. 3D ultrasound biomicroscopy (3D-UBM) imag-

ing and automated 3D assessment of the iridocorneal angle for glaucoma patients. In: *Medical Imaging 2019: Ultrasonic Imaging and Tomography*. Vol. 10955. Bellingham, WA: SPIE; 2019:109550U.

24. Volpe NJ. Adler's physiology of the eye: clinical application. *J Neuroophthalmol*. 2004;24(4): 348.
25. Xiao J, Tan Y, Li W, et al. Tumor volume reduction rate is superior to RECIST for predicting the pathological response of rectal cancer treated with neoadjuvant chemoradiation: results from a prospective study. *Oncol Lett*. 2015;9(6):2680–2686.

Supplementary Materials

Supplementary Movie S1. Anterior and posterior iris in ex vivo human eye. Interactive 3D view allow rotations and cropping to create unobstructed view of the relevant structures i.e., ciliary muscle and individual ciliary processes.

Supplementary Movie S2. Placement of Acrysof single piece IOL and haptics (blue) in 360º around the eye. In addition to 3D visualization, 3D-UBM allows traditional 2D visualization of the IOL and information on lens position relative to the posterior iris, ciliary processes and the capsular bag around the entire globe.